Stability of the Boundary Layer on a Spinning Semi-Infinite Circular Cylinder

Kai-Hsiung Kao* and Chuen-Yen Chow†
University of Colorado, Boulder, Colorado 80309

The incompressible laminar velocity field in the boundary layer along a semi-infinite circular cylinder is computed numerically. Being aligned with a uniform oncoming flow, the cylinder may have a constant spin motion about its axis. A linear stability analysis of the boundary layer is carried out employing the Chebyshev collocation spectral method, which can be used to predict both the location at which the onset of instability occurs and the mode of the disturbance to be first excited. Results show that the transverse curvature of the cylinder has a stabilizing effect and the spin motion destabilizes the flow by shifting the onset of instability in the upstream direction.

Nomenclature

c = complex phase velocity
$D_{jk}^{(p)}$ = Chebyshev collocation matrices
f = nondimensional stream function
g = nondimensional velocity in the azimuthal direction
I = identiy matrix
i = $\sqrt{-1}$, imaginary unit
N = number of grid points
N' = order of the Chebyshev expansion
n = integer wave number in the azimuthal direction
p' = unsteady small perturbed pressure
Re = Reynolds number based on the characteristic length, $\sqrt{u_\infty x/\nu}$
Re_{r_o} = Reynolds number based on the radius of cylinder
r = radial distance from the center of cylinder
r_o = constant radius of the cylinder
s = nondimensional spin rate
T_k = Chebyshev polynomials
t = time
U,W = steady mean velocities
u_∞ = freestream velocity
u,v,w = total velocity components
u',v',w' = unsteady small perturbed velocities
$\tilde{u},\tilde{v},\tilde{w},\tilde{p}$ = complex eigenfunctions
w_w = azimuthal velocity of the cylinder surface
x = axial distance from the leading edge
Y = transformation parameter
α = wave number in the axial direction, real
θ = azimuthal angle
ν = kinematic viscosity of the fluid
ξ,η = transformed variables
ψ = dimensional stream function

Subscript

$(\,)_{tr}$ = value at onset of instability

Superscript

$(\tilde{\ })$ = transformed quantity

I. Introduction

IT has been observed in the laboratory that the transition from laminar to turbulent flow in the boundary layer along a cylindrical body initiates in the form of two-dimensional Tollmien-Schlichting waves, followed by a region dominated by three-dimensional stretching of vortex lines that leads to the final breakdown of the flow into a chaotic state. Boundary layers on spinning and nonspinning axisymmetric bodies exhibit different modes of instability that depend on transverse curvature and spin rate. For axisymmetric bodies without spin, a two- or three-dimensional viscosity-conditioned instability leads to the development of Tollmien-Schlichting waves and their breakdown. On the other hand, for spinning bodies, an inflectional crossflow instability generates vortices that spiral around the spinning body and break down, possibly after a helical instability. Each of these modes appears to possess distinct topology of nonlinear breakdown and onset of turbulence. The purpose of the present work is to study numerically the stability properties of the boundary layer on a semi-infinitely long circular cylinder by varying the cylinder radius or the spin rate.

On the boundary layers along bodies of revolution, the effects of transverse curvature have been investigated by several authors. Young[1] and Jacob and Dow[2] used approximate techniques to compute the velocity profiles without and with heat transfer, respectively. Seban and Bond[3] solved the problem using a power series valid close to the leading edge. Glauert and Lighthill[4] used the Polhausen method to obtain results both near the leading edge and far downstream, and Stewartson[5] studied the effect of compressibility. Jaffe and Okamura[6] computed the flow over a range that began at the leading edge and extended far downstream using an explicit finite-difference method. However, for the case of a cylinder with a blunt nose, Smith and Clutter[7] pointed out that the solution may fail to converge at the outer region of the boundary layer by applying an explicit integral scheme. Thus, to avoid the numerical instability, implicit methods have been suggested[8] for solving the boundary-layer equations.

The nature of the instability mechanism in axisymmetric boundary layers has been examined experimentally, for example, by Brown,[9] Knapp and Roache,[10] and Kegelman et al.[11] Morris and Byon[12] made a calculation for the stability of a boundary layer on a circular cylinder. However, they restricted the analysis to that for axisymmetric disturbance only and did not obtain the neutral stability curves. Although there is no difficulty in deriving the linearized perturbation equations for

Presented as Paper 90-0116 at the AIAA 28th Aerospace Sciences Meeting, Reno, NV, Jan. 8–11, 1990; received Feb. 17, 1990; revision received Aug. 6, 1990; accepted for publication Aug. 15, 1990.

*Research Associate, Aerospace Engineering Sciences. Member AIAA.

†Professor, Aerospace Engineering Sciences. Associate Fellow AIAA.

general nonaxisymmetric disturbances, the resulting equations are extremely complicated and cannot be reduced, by a transformation of Squire's type, to an equivalent axisymmetric problem. The Chebyshev collocation spectral method enables the perturbation equations to be solved accurately and efficiently. The method has been employed in the plane Poiseuille flow and Blasius flow problems[13] to obtain highly accurate solutions. The eigenvalue problems of hydrodynamic stability are often difficult because they usually require the solution of nearly singular boundary value problems. It is desirable to use the Chebyshev collocation spectral method[14,15] because of the following advantages: 1) it has good convergence properties,[13] and 2) derivatives can be calculated by analytical differentiation of the functions used, which can therefore be differentiated as often as desired to substantially exclude the effect of numerical dissipation.

As long as the boundary-layer thickness is small compared with the body radius, the plane stability results may be used with confidence and also the Squire's theorem exists. However, if the boundary-layer thickness is of the order of the cylinder radius, then the transverse curvature effect must be accounted for. Furthermore, spin motion induces a centrifugal instability on large-curvature cylinders, or a crossflow instability on small-curvature cylinders, and, thus, may dramatically change the boundary-layer transition characteristics. As a validation of the numerical procedure, comparisons are made between the present result for a large cylinder radius and that for a flat plate boundary layer obtained by Jordinson.[16]

II. Analysis

This section gives a description of both the basic laminar boundary-layer solution and the linearized stability analysis.

Laminar Boundary Layer

For incompressible laminar flow over a circular cylinder, a sketch of the coordinate system is shown in Fig. 1. The equations governing the steady, thin and axisymmetric boundary layer in cylindrical coordinates are as follows:

$$\frac{\partial}{\partial x}(ru)+\frac{\partial}{\partial r}(rv)=0 \tag{1}$$

$$v\frac{\partial u}{\partial r}+u\frac{\partial u}{\partial x}=\nu\left(\frac{\partial^2 u}{\partial r^2}+\frac{1}{r}\frac{\partial u}{\partial r}\right) \tag{2}$$

$$v\frac{\partial w}{\partial r}+\frac{vw}{r}+u\frac{\partial w}{\partial x}=\nu\left(\frac{\partial^2 w}{\partial r^2}+\frac{1}{r}\frac{\partial w}{\partial r}-\frac{w}{r^2}\right), \tag{3}$$

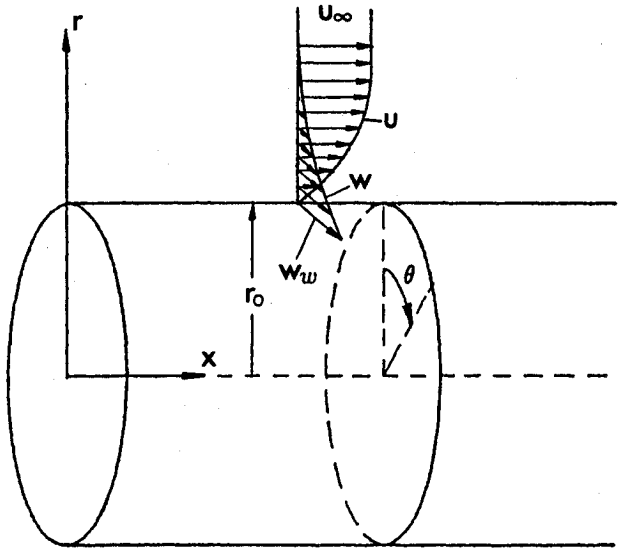

Fig. 1 Coordinate system and a sketch of the boundary layer on a circular cylinder.

where w is generated by the body spin motion. It was found that, for the simultaneous rotation and forced flow, there exists no similarity transformation to reduce the partial differential equations to ordinary ones. Nevertheless, the following similarity-type transformations making use of the stream function can still be used,

$$u=\frac{1}{r}\frac{\partial\psi}{\partial r} \tag{4a}$$

$$v=-\frac{1}{r}\frac{\partial\psi}{\partial x} \tag{4b}$$

$$\xi=\frac{4}{r_o}\left(\frac{\nu x}{u_\infty}\right)^{1/2} \tag{4c}$$

$$\eta=\left[\frac{r^2-r_o^2}{4r_o}\right]\left(\frac{u_\infty}{\nu x}\right)^{1/2} \tag{4d}$$

$$f=\frac{\psi}{r_o}(u_\infty \nu x)^{-1/2} \tag{4e}$$

$$g=\frac{w}{u_\infty} \tag{4f}$$

For a given x, the numerical value of ξ is proportional to the ratio of the local boundary-layer thickness and the radius of the cylinder. By manipulating Eqs. (4a–f), the velocity components can be written as

$$u=\left(\frac{u_\infty}{2}\right)f' \tag{5}$$

$$v=\frac{1}{2}\frac{r_o}{r}\left(\frac{\nu u_\infty}{x}\right)^{1/2}(\eta f'-f)-\frac{2\nu}{r}\frac{\partial f}{\partial\xi} \tag{6}$$

$$w=u_\infty g \tag{7}$$

where the superscript prime denotes partial differentiation with respect to η. Upon substitution of Eqs. (5–7), the governing differential equations (2) and (3) become

$$(1+\xi\eta)f'''+\xi f''+ff''=\xi\left(f'\frac{\partial f'}{\partial\xi}-f''\frac{\partial f}{\partial\xi}\right) \tag{8}$$

$$(1+\xi\eta)g''=-(f+\xi)g'+\frac{\xi^2+2\xi(\eta f'-f)}{4(1+\xi\eta)}g$$

$$-\frac{\partial f}{\partial\xi}\left[\xi g'+\frac{\xi^2}{2(1+\xi\eta)}g\right]+\frac{\partial g}{\partial\xi}\xi f' \tag{9}$$

In terms of the transformed coordinates (ξ,η), the boundary conditions are

$$f(\xi,0)=f'(\xi,0)=0 \tag{10a}$$

$$g(\xi,0)=\frac{w_w}{u_\infty}\equiv s \tag{10b}$$

$$f'(\xi,\infty)=2 \tag{11a}$$

$$g(\xi,\infty)=0 \tag{11b}$$

where s is the ratio of the tangential velocity of the cylinder surface to the freestream velocity.

Linear Stability Analysis

To investigate the stability of the boundary layer, the flow is decomposed into a steady mean field (U,W) and an unsteady small perturbed field (u',v',w',p'). Substitution of

those quantities into the unsteady equations of motion results in the following linearized equations:

$$\frac{\partial v'}{\partial r} + \frac{v'}{r} + \frac{1}{r}\frac{\partial w'}{\partial \theta} + \frac{\partial u'}{\partial x} = 0 \tag{12a}$$

$$\frac{\partial u'}{\partial t} + v'\frac{\partial U}{\partial r} + U\frac{\partial u'}{\partial x} + \frac{W}{r}\frac{\partial u'}{\partial \theta} = -\frac{\partial p'}{\partial x} + \frac{1}{Re}\left[\frac{\partial^2 u'}{\partial r^2} + \frac{1}{r}\frac{\partial u'}{\partial r} + \frac{1}{r^2}\frac{\partial^2 u'}{\partial \theta^2} + \frac{\partial^2 u'}{\partial x^2}\right] \tag{12b}$$

$$\frac{\partial v'}{\partial t} + U\frac{\partial v'}{\partial x} + \frac{W}{r}\frac{\partial v'}{\partial \theta} - \frac{2Wv'}{r} = -\frac{\partial p'}{\partial r} + \frac{1}{Re}\left[\frac{\partial^2 v'}{\partial r^2} + \frac{1}{r}\frac{\partial v'}{\partial r} - \frac{v'}{r^2} + \frac{1}{r^2}\frac{\partial^2 v'}{\partial \theta^2} - \frac{2}{r^2}\frac{\partial w'}{\partial \theta} + \frac{\partial^2 v'}{\partial x^2}\right] \tag{12c}$$

$$\frac{\partial w'}{\partial t} + U\frac{\partial w'}{\partial x} + v'\frac{\partial W}{\partial r} + \frac{W}{r}\frac{\partial w'}{\partial \theta} + \frac{Wv'}{r} = -\frac{1}{r}\frac{\partial p'}{\partial \theta} + \frac{1}{Re}\left[\frac{\partial^2 w'}{\partial r^2} + \frac{1}{r}\frac{\partial w'}{\partial r} - \frac{w'}{r^2} + \frac{1}{r^2}\frac{\partial^2 w'}{\partial \theta^2} + \frac{2}{r^2}\frac{\partial v'}{\partial \theta} + \frac{\partial^2 w'}{\partial x^2}\right] \tag{12d}$$

in which U and W are solutions of Eqs. (8) and (9), and

$$Re = \frac{u_\infty\sqrt{\nu x/u_\infty}}{\nu} = \sqrt{\frac{u_\infty x}{\nu}} \tag{13}$$

is the Reynolds number proportional to the boundary-layer thickness. The fluctuations are assumed to have the Fourier forms

$$u' = \hat{u}(r)\cdot\exp[i\alpha(x-ct)+in\theta] \tag{14a}$$

$$v' = \hat{v}(r)\cdot\exp[i\alpha(x-ct)+in\theta] \tag{14b}$$

$$w' = \hat{w}(r)\cdot\exp[i\alpha(x-ct)+in\theta] \tag{14c}$$

$$p' = \hat{p}(r)\cdot\exp[i\alpha(x-ct)+in\theta] \tag{14d}$$

where $n=0$ represents an axisymmetric perturbation and a positive n represents a disturbance wave propagating at an angle $\varphi=\tan^{-1}(n/\alpha)$ to the axial direction in the quadrant plane formed by the positive axial and positive spinwise directions. On the other hand, a disturbance propagating in the opposite direction is represented by a negative n. Substitution of Eqs. (14a–d) in the linearized equations yields

$$i\alpha\hat{u} + \hat{v}' + \frac{1}{r}\hat{v} + \frac{in}{r}\hat{w} = 0 \tag{15a}$$

$$i\alpha(U-c)\hat{u} + U'\hat{v} + i\alpha\hat{p} + i\frac{nW}{r}\hat{u} = \frac{1}{Re}\left[\hat{u}'' + \frac{1}{r}\hat{u}' - \left(\alpha^2 + \frac{n^2}{r^2}\right)\hat{u}\right] \tag{15b}$$

$$i\alpha(U-c)\hat{v} + \hat{p}' + \frac{W}{r}(in\hat{v} - 2\hat{w}) = \frac{1}{Re}\left[\hat{v}'' + \frac{1}{r}\hat{v}' - \left(\alpha^2 + \frac{n^2+1}{r^2}\right)\hat{v} - i\frac{2n}{r^2}\hat{w}\right] \tag{15c}$$

$$i\alpha(U-c)\hat{w} + \frac{in}{r}\hat{p}' + \left(W' + \frac{W}{r}\right)\hat{v} + i\frac{nW}{r}\hat{w} = \frac{1}{Re}\left[\hat{w}'' + \frac{1}{r}\hat{w}' - \left(\alpha^2 + \frac{n^2+1}{r^2}\right)\hat{w} + i\frac{2n}{r^2}\hat{v}\right] \tag{15d}$$

whose boundary conditions are

$$\hat{u}(r_o) = \hat{v}(r_o) = \hat{w}(r_o) = 0 \tag{16a}$$

$$\hat{u}(\infty) = \hat{v}(\infty) = \hat{w}(\infty) = \hat{p}(\infty) = 0 \tag{16b}$$

Using Eqs. (4c) and (4d), the perturbation equations (15a–d) are transformed into the computational domain (ξ,η),

$$i\alpha\hat{u} + \zeta^{1/2}\hat{v}' + \frac{\xi}{8\zeta^{1/2}}\hat{v} + \frac{in\xi}{8\zeta^{1/2}}\hat{w} = 0 \tag{17a}$$

$$i\alpha(U-c)\hat{u} + \zeta^{1/2}U'\hat{v} + i\alpha\hat{p} + i\frac{n\xi W}{8\zeta^{1/2}}\hat{u} = \frac{1}{Re}\left[\zeta\hat{u}'' + \frac{\xi}{4}\hat{u}' - \left(\alpha^2 + \frac{n^2\xi^2}{64\zeta}\right)\hat{u}\right] \tag{17b}$$

$$i\alpha(U-c)\hat{v} + \zeta^{1/2}\hat{p}' + \frac{\xi W}{8\zeta^{1/2}}(in\hat{v} - 2\hat{w}) = \frac{1}{Re}\left\{\zeta\hat{v}'' + \frac{\xi}{4}\hat{v}' - \left[\alpha^2 + \frac{(n^2+1)\xi^2}{64\zeta}\right]\hat{v} - i\frac{2n\xi^2}{64\zeta}\hat{w}\right\} \tag{17c}$$

$$i\alpha(U-c)\hat{w} + i\frac{n\xi}{8\zeta^{1/2}}\hat{p} + \left(\zeta^{1/2}W' + \frac{\xi W}{8\zeta^{1/2}}\right)\hat{v} + i\frac{n\xi W}{8\zeta^{1/2}}\hat{w} = \frac{1}{Re}\left\{\zeta\hat{w}'' + \frac{\xi}{4}\hat{w}' + \left[\alpha^2 + \frac{(n^2+1)\xi^2}{64\zeta}\right]\hat{w} + i\frac{2n\xi^2}{64\zeta}\hat{v}\right\} \tag{17d}$$

where the primes represent derivatives with respect to η, and ζ is a combined quantity, defined as $(1+\xi\eta)/4$. Boundary conditions (16a) and (16b) then become

$$\hat{u}(0) = \hat{v}(0) = \hat{w}(0) = 0 \tag{18a}$$

$$\hat{u}(\infty) = \hat{v}(\infty) = \hat{w}(\infty) = \hat{p}(\infty) = 0 \tag{18b}$$

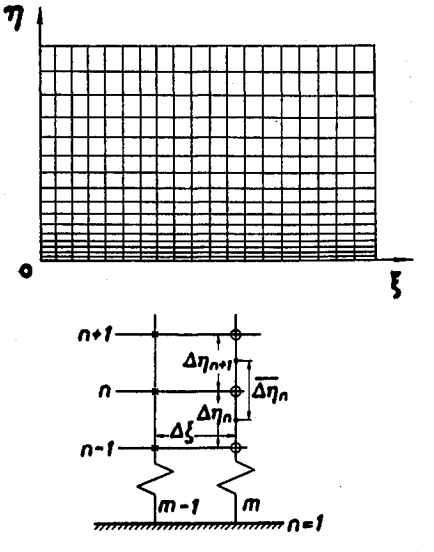

Fig. 2 Schematic of the computational grid system.

III. Method of Solution

In the boundary layer along a cylinder of constant radius, the axial velocity is not affected by the tangential velocity, as indicated by Eqs. (2) and (8). Thus, the tangential velocity is computed by solving Eq. (9) for g after the solution for f has been obtained from Eq. (8). An implicit method is used for the computation to avoid the possible numerical instability in the outer region of the boundary layer for a nonsimilar flow. On the other hand, a linearized stability analysis of the flow is carried out by employing the Chebyshev collocation spectral method.

Implicit Method for Computating the Mean Flow

Equation (8) is first reduced to a set of ordinary differential equations by using an approximate representation of the derivatives with respect to ξ, which are of first order and appear only on the right side of the equation.

The boundary-layer flow is computed by marching in the direction of increasing ξ. At any station m, the quantities $(\partial f/\partial \xi)_m$ and $(\partial f'/\partial \xi)_m$ are approximated in terms of the values of f and f' at the local and previous stations. At the zeroth station, the right side of Eq. (8) vanishes since $\xi_o = 0$, and derivatives with respect to ξ are not needed so that the equation reduces to that for the Blasius flow.

It is more convenient to reduce Eq. (8) to second order. To this end, the variable $F = f'$ is introduced and Eq. (8) is rewritten as

$$(1+\xi\eta)F_{\eta\eta} + \xi F_\eta + fF_\eta = \xi(FF_\xi - f_\xi F_\eta) \tag{19}$$

The two variables f and F in this equation are related through the expression

$$f(\xi,\eta) = \int_0^\eta F(\xi,\eta)\, d\eta + f(\xi,0) \tag{20}$$

The boundary conditions are

$$F(\xi,0) = f(\xi,0) = 0 \tag{21a}$$

$$F(\xi,\infty) = 2 \tag{21b}$$

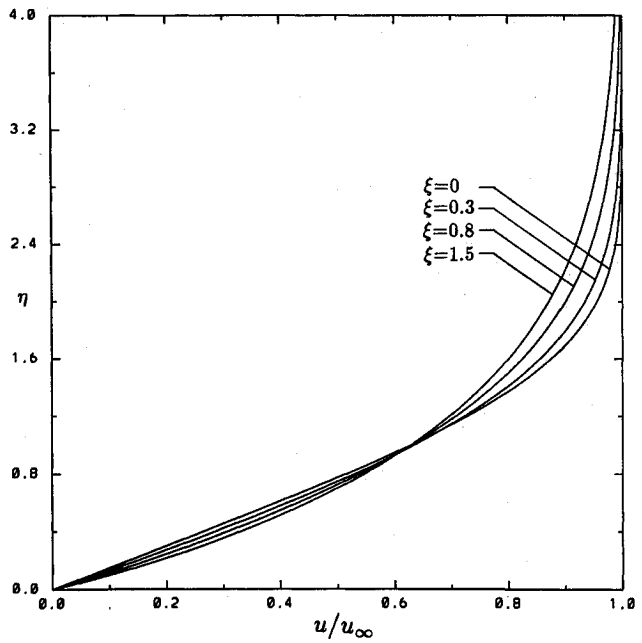

Fig. 3 Axial velocity profiles for different values of ξ on nonspinning cylinder.

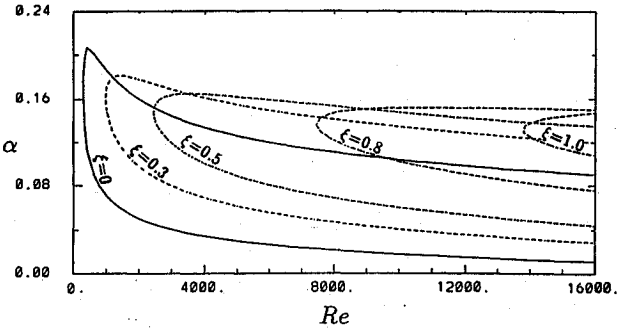

Fig. 4 Neutral stability curves for axisymmetric disturbances.

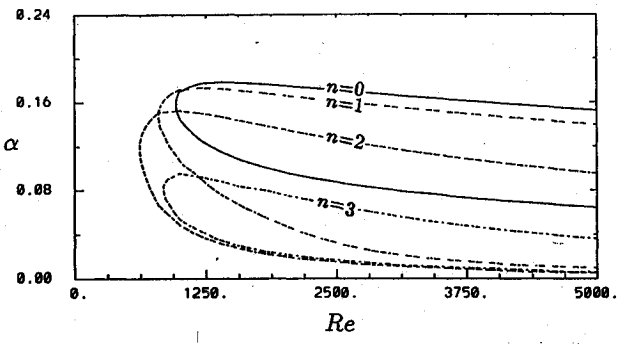

Fig. 5 Neutral stability curves for axisymmetric and nonaxisymmetric disturbances at $\xi = 0.3$ (critical condition is determined by the $n = 2$ curve).

A variable size grid in the η direction is adopted to handle the boundary layers characterized by large thickness, which permits shorter steps close to the wall to maintain computing accuracy. A small $\Delta\xi$ of 0.015 is used near $\xi = 0$ to avoid divergence of the solution. Thereafter, the size of $\Delta\xi$ does not need to be so small, but the same small value has been used in the present computation. The schematic of the grid system is shown in Fig. 2. Central-difference approximations to the derivatives F_η and $F_{\eta\eta}$ at ξ_m are obtained by expanding $F_{m,n+1}$ and $F_{m,n-1}$ in Taylor series about (m,n). Thus, Eq. (19) becomes

$$A_n F_{m,n-1} + B_n F_{m,n} + C_n F_{m,n+1} = D_n \tag{22}$$

which represents a set of $N-2$ simultaneous algebraic equations at each station m for the unknowns $F_{m,n}$ ($n = 2,3,4,\ldots, N-1$).

Finally, Eq. (22) is rewritten in the standard form with subscripts m omitted,

$$A_n F_{n-1} + B_n F_n + C_n F_{n+1} = D_n, \quad 2 \le n \le N-1 \tag{23}$$

The boundary conditions are

$$F_1 = 0, \qquad F_N = 2 \tag{24}$$

where $n = 1$ denotes the wall and $n = N$ the edge of the boundary layer. A solution procedure justified by Richtmeyer[17] is applied to solve Eq. (23) with boundary conditions (24). Once $F_{m,n}$ have been determined, the corresponding solution for $f_{m,n}$ can be found by direct numerical integration of Eq. (20).

The calculated values of $F_{m,n}$ and $f_{m,n}$ are used to determine the new values of the coefficients A_n, B_n, C_n, and D_n, which in turn leads to a set of improved values of $F_{m,n}$ and $f_{m,n}$. The process is repeated until the results of two successive iterations agree to within a specified tolerance, typically of order 10^{-6}.

After the solution f of Eq. (8) has been computed, Eq. (9) is then solved with boundary conditions (10) and (11) using a similar procedure to obtain the tangential velocity distribution.

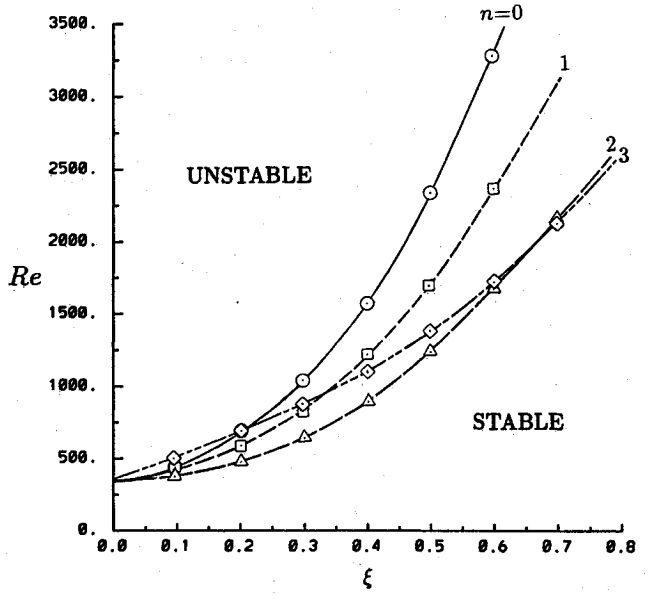

Fig. 6 Curves of the lowest Reynolds number vs the curvature factor ξ for axisymmetric and nonaxisymmetric disturbances, whose lower envelope is defined as the critical curve.

Chebyshev Collocation Spectral Method for Stability Analysis

The stability problem has been reduced to solving an eigenvalue problem formed by Eqs. (17a–d) and boundary conditions (18a) and (18b). As a first step, the semi-infinite range of η between 0 and ∞ is transformed by using the transformation

$$\tilde{\eta} = \exp(-\eta/Y) \tag{25}$$

onto the interval between 1 and 0 of the transformed variable, where $Y>0$ is a scaling parameter.

Any function $\phi(\tilde{\eta})$ in the computational domain, which can be $\hat{u}$, $\hat{v}$, $\hat{w}$, or $\hat{p}$ in Eqs. (17a–d), is expanded in a Chebyshev series after the transformation (25),

$$\phi(\tilde{\eta}) = \sum_{k=0}^{N'} \tilde{\phi}_k T_k(\tilde{\eta}) \tag{26}$$

Since the Chebyshev polynomials

$$T_k(\tilde{\eta}) = \cos\left[k \cdot \arccos(\tilde{\eta})\right] \tag{27}$$

are defined in $-1 \le \tilde{\eta} \le 1$, the function $\phi(\tilde{\eta})$ is extended to the interval between -1 and 0 by defining

$$\phi(\tilde{\eta}) = 0, \qquad -1 \le \tilde{\eta} < 0 \tag{28}$$

Instead of calculating the coefficients $\tilde{\phi}_k$ in Eq. (26) directly, we use the Chebyshev matrix collocation method. To calculate derivatives, values of the functions at the collocation points

$$\tilde{\eta}_j = \cos(\pi j/N'), \qquad j = 0,1,\ldots,N' \tag{29}$$

are used. The derivatives $\phi^{(p)}(\tilde{\eta}_j)$ are obtained from the matrix multiplication

$$\phi^{(p)}(\tilde{\eta}_j) = \sum_{k=0}^{N'} D_{jk}^{(p)} \phi(\tilde{\eta}_k), \qquad j = 0,1,\ldots,N' \tag{30}$$

Thus, the collocation matrices, which depend only on N', are generated by the following formulas

$$D_{jk}^{(1)} = \frac{\bar{c}_j}{\bar{c}_k} \frac{(-1)^{j+k}}{\tilde{\eta}_j - \tilde{\eta}_k}, \qquad j \ne k \tag{31a}$$

$$D_{jj}^{(1)} = -\frac{\tilde{\eta}_j}{2(1-\tilde{\eta}_j^2)}, \qquad j \le N' \tag{31b}$$

$$D_{oo}^{(1)} = \frac{2N'^2+1}{6} = -D_{N'N'}^{(1)} \tag{31c}$$

where

$$\bar{c}_o = \bar{c}_{N'} = 2$$

$$\bar{c}_j = 1, \qquad j \ne 0 \quad \text{or} \quad N'$$

$$D_{jk}^{(p)} = \left[D_{jk}^{(1)}\right]^p \tag{32}$$

The matrix collocation method is now modified for the η interval so that derivatives with respect to η can be directly calculated within this interval. There are N number of collocation points within the interval $0 \le \tilde{\eta} \le 1$ after the inverse transformation. They are

$$\eta_j = -Y \ell n(\tilde{\eta}_j), \qquad j = 0,1,\ldots,N-1 \tag{33}$$

in which

$$N = \frac{N'+1}{2}, \qquad \text{for } N' \text{ odd} \tag{34a}$$

$$N = \frac{N'}{2}, \qquad \text{for } N' \text{ even} \tag{34b}$$

Equation (30) becomes, after transformation into the η interval,

$$\phi^{(p)}(\eta_j) = \sum_{k=0}^{N-1} \tilde{D}_{jk}^{(p)} \phi(\eta_k) \tag{35}$$

The transformed matrix and the matrices $\tilde{D}_{jk}^{(p)}$ for higher derivatives, $p>1$, are calculated by using the chain rule as

$$\tilde{D}_{jk}^{(1)} = D_{jk}^{(1)} \cdot \tilde{\eta}_{(\eta)}^{(1)} \tag{36a}$$

$$\tilde{D}_{jk}^{(2)} = D_{jk}^{(2)} \cdot \left[\tilde{\eta}_{(\eta)}^{(1)}\right]^2 + D_{jk}^{(1)} \cdot \tilde{\eta}_{(\eta)}^{(2)} \tag{36b}$$

$$\tilde{D}_{jk}^{(3)} = D_{jk}^{(3)} \cdot \left[\tilde{\eta}_{(\eta)}^{(1)}\right]^3 + 3D_{jk}^{(2)} \cdot \tilde{\eta}_{(\eta)}^{(1)} \cdot \tilde{\eta}_{(\eta)}^{(2)} + D_{jk}^{(1)} \cdot \tilde{\eta}_{(\eta)}^{(3)} \tag{36c}$$

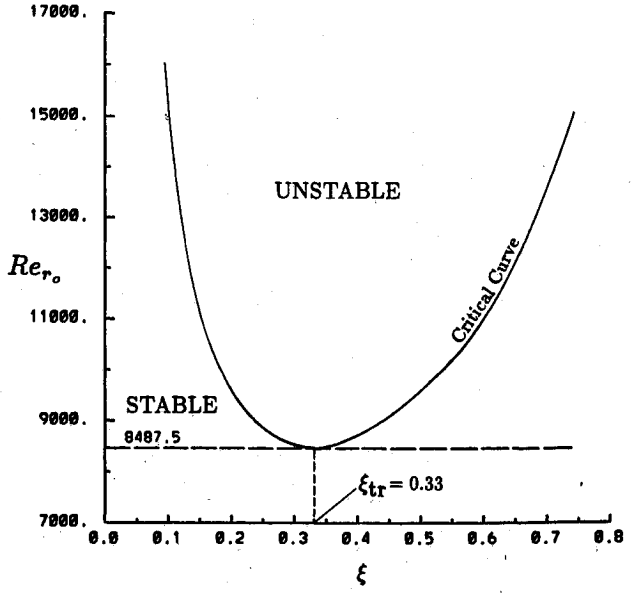

Fig. 7 Critical curve of the Reynolds number based on cylinder radius.

$$\tilde{D}^{(4)}_{jk} = D^{(4)}_{jk}\cdot\left[\tilde{\eta}^{(1)}_{(\eta)}\right]^4 + 6D^{(3)}_{jk}\cdot\left[\tilde{\eta}^{(1)}_{(\eta)}\right]^2\cdot\tilde{\eta}^{(2)}_{(\eta)} + D^{(2)}_{jk}\left\{3\cdot\left[\tilde{\eta}^{(2)}_{(\eta)}\right]^2 + 4\cdot\tilde{\eta}^{(1)}_{(\eta)}\cdot\tilde{\eta}^{(3)}_{(\eta)}\right\} + D^{(1)}_{jk}\cdot\tilde{\eta}^{(4)}_{(\eta)} \tag{36d}$$

where

$$\tilde{\eta}^{(p)}_{(\eta)} = \frac{\partial^p\tilde{\eta}}{\partial\eta^p} = (-1)^p Y^{-p}\exp\left(-\frac{\eta}{Y}\right) \tag{37}$$

In terms of the collocation matrices, the perturbation equations (17a–d) are expressed in the following form:

$$[i\alpha I]\hat{u} + \left[\zeta^{1/2}\tilde{D}^{(1)} + \frac{\xi I}{8\zeta^{1/2}}\right]\hat{v} + \left[i\frac{n\xi I}{8\zeta^{1/2}}\right]\hat{w} = 0 \tag{38a}$$

$$\left\{UI + \frac{n\xi WI}{8\alpha\zeta^{1/2}} + \frac{i}{\alpha Re}\left[\zeta\tilde{D}^{(2)} + \frac{\xi}{4}\tilde{D}^{(1)} - \alpha^2 I - \frac{n^2\xi^2 I}{64\zeta}\right]\right\}\hat{u} - \left[i\frac{\zeta^{1/2}U'I}{\alpha}\right]\hat{v} + I\hat{p} - cI\hat{u} = 0 \tag{38b}$$

$$\left\{UI + \frac{n\xi WI}{8\alpha\zeta^{1/2}} + \frac{i}{\alpha Re}\left[\zeta\tilde{D}^{(2)} + \frac{\xi}{4}\tilde{D}^{(1)} - \alpha^2 I - \frac{(n^2+1)\xi^2 I}{64\zeta}\right]\right\}\hat{v} + \left[i\frac{\xi WI}{4\alpha\zeta^{1/2}} + \frac{n\xi^2 I}{32\alpha Re\,\zeta}\right]\hat{w} - \left[i\frac{\zeta^{1/2}\tilde{D}^{(1)}}{\alpha}\right]\hat{p} - cI\hat{v} = 0 \tag{38c}$$

$$\left[-\frac{i}{\alpha}\left(\zeta^{1/2}W'I + \frac{\xi WI}{8\zeta^{1/2}}\right) - \frac{n\xi^2 I}{32\alpha Re\,\zeta}\right]\hat{v} + \left\{UI + \frac{n\xi WI}{8\alpha\zeta^{1/2}} + \frac{i}{\alpha Re}\left[\zeta\tilde{D}^{(2)} + \frac{\xi}{4}\tilde{D}^{(1)} - \alpha^2 I - \frac{(n^2+1)\xi^2 I}{64\zeta}\right]\right\}\hat{w} + \left[\frac{n\xi I}{8\alpha\zeta^{1/2}}\right]\hat{p} - cI\hat{w} = 0 \tag{38d}$$

A block-generalized eigenvalue system is thus obtained,

$$\begin{bmatrix}[A_{11}] & [A_{12}] & [A_{13}] & [A_{14}]\\ [A_{21}] & [A_{22}] & [A_{23}] & [A_{24}]\\ [A_{31}] & [A_{32}] & [A_{33}] & [A_{34}]\\ [A_{41}] & [A_{42}] & [A_{43}] & [A_{44}]\end{bmatrix}\begin{bmatrix}[\hat{u}]\\ [\hat{v}]\\ [\hat{w}]\\ [\hat{p}]\end{bmatrix} = [c]\begin{bmatrix}[B_{11}] & [B_{12}] & [B_{13}] & [B_{14}]\\ [B_{21}] & [B_{22}] & [B_{23}] & [B_{24}]\\ [B_{31}] & [B_{32}] & [B_{33}] & [B_{34}]\\ [B_{41}] & [B_{42}] & [B_{43}] & [B_{44}]\end{bmatrix}\begin{bmatrix}[\hat{u}]\\ [\hat{v}]\\ [\hat{w}]\\ [\hat{p}]\end{bmatrix} \tag{39}$$

where both $[A]$ and $[B]$ are $4N\times 4N$ matrices, and c is the eigenvalue diagonal matrix. In the eigenvalue system, $[\hat{u}]$, $[\hat{v}]$, $[\hat{w}]$, and $[\hat{p}]$ represent the eigenfunctions of the velocity and pressure fluctuations, respectively.

IV. Results and Discussion

In the present analysis, only the temporal stability characteristics are examined. The results for the stability of laminar boundary layers on a constant-radius cylinder with and without spin are presented separately.

Nonspinning Cylinder

The axial velocity profiles computed for various values of ξ are plotted in Fig. 3. According to the definition [Eq. (4c)] of ξ, they represent either the velocity profiles at different stations along a semi-infinitely long cylinder of a given radius or those at a fixed distance from the leading edge on cylinders having different radii, with $\xi = 0$ representing the Blasius velocity profile for the similar boundary layer on a flat plate. Figure 3 shows that the effect of increasing the transverse curvature by reducing the cylinder radius is to make the velocity profile fuller near the cylinder and less steep at the edge of the boundary layer, leading to a higher shear stress at the wall.

Without any computational instabilities, the velocity profiles obtained here using an implicit method agree in appearance with those obtained by Jaffe and Okamura[6] using an explicit method. Although a direct comparison cannot be made because of the unavailability of numerical data describing the velocity profiles in Ref. 6, a maximum difference of only 1.2% in skin friction values is found between the two sets of solutions.

Stability analyses of the velocity profiles shown in Fig. 3 are then performed. To test the accuracy of the present computational procedure, a case for $n = 0$ and $\xi = 0$ is used in which $Re = 5.8\times 10^2$, $\alpha = 0.179$, $Y = 5$, and $N = 31$. The complex eigenvalues of c so computed agree very well with those obtained by Laurien[13] under the same conditions but using a different numerical procedure. It requires approximately 0.2 s on Cyber 205 for such a single run.

For given n and ξ, the results of the stability analysis are presented in the α vs Re diagram in the form of constant c_i curves. Among those curves, the locus $c_i = 0$, which separates the region of stable from that of unstable disturbances, is called the curve of neutral stability. For the axisymmetric mode $n = 0$, the neutral stability curves are plotted in Fig. 4 for different values of ξ. The $\xi = 0$ curve shows that the critical Reynolds number is 3.07×10^2, above which the axisymmetric disturbances are amplified and the flow becomes unstable. This value is equivalent to a critical Reynolds number of 5.28×10^2 based on the boundary-layer thickness. The close agreement with the value 5.2×10^2 obtained by Jordinson[16] for the flat plate boundary layer serves again as a check for the accuracy of the present method. The phenomenon that the critical Reynolds number increases with increasing ξ indicates that the transverse curvature has a stabilizing effect on axisymmetric disturbances.

Figure 5 shows the neutral stability curves for the first three nonaxisymmetric modes as compared with that for the axisymmetric mode, all computed for $\xi = 0.3$. It reveals that, at this nonvanishing value of ξ, $n = 0$ is no longer the most unstable

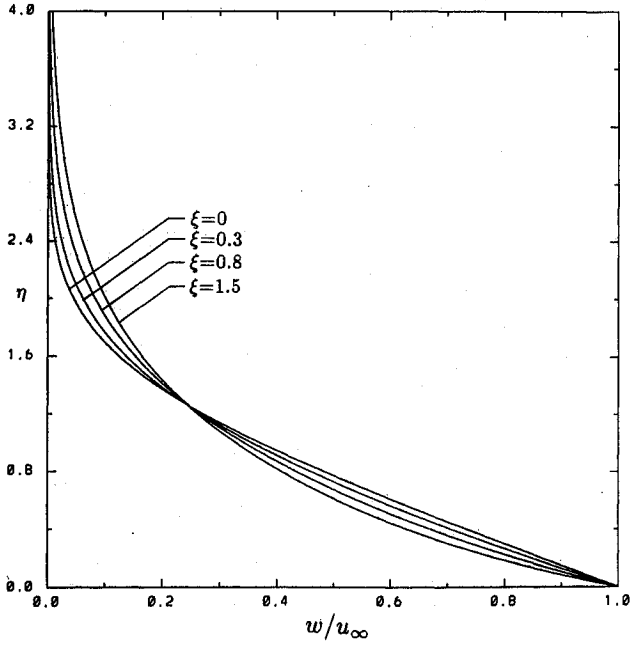

Fig. 8 Tangential velocity profiles for various values of ξ on a spinning cylinder with $s = 1$.

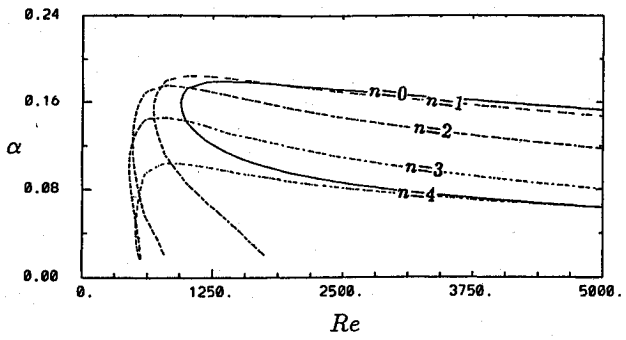

Fig. 9 Neutral stability curves for axisymmetric and nonaxisymmetric disturbances at $\xi = 0.3$ with $s = 0.05$ (critical condition occurs on the $n = 3$ curve).

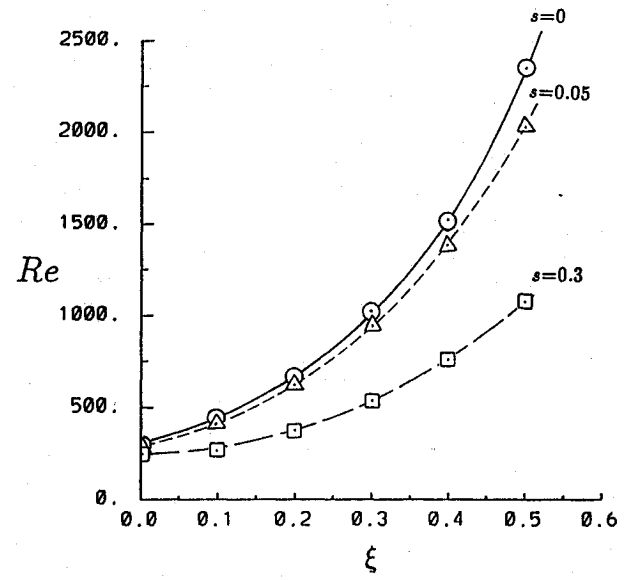

Fig. 10 Curves of the lowest Reynolds numbers for $n = 0$ with different spin rates.

mode so that Squire's theorem may not be valid for flow with a transverse curvature.

The critical Reynolds numbers for $n \leq 3$ are plotted against ξ in Fig. 6, showing that the transverse curvature has also a stabilizing effect on each of those nonaxisymmetric disturbances. For a given ξ, each mode has its own critical Reynolds number. The lowest among all critical values is defined as the critical Reynolds number of the boundary layer at that particular ξ, which is represented by the lower envelope of all curves shown in Fig. 6. Note that the most unstable mode varies along this critical curve; it changes from $n = 0$ for ξ close to zero to $n = 2$ for ξ up to around 0.67, and changes again to $n = 3$ as ξ increases further, and so forth.

Since Re and ξ are both functions of x, it is sometimes more convenient to plot the critical curve alternatively in the Re_{r_o} vs ξ diagram, as shown in Fig. 7, where $Re_{r_o} = u_\infty r_o/\nu$ is related to Re through the equation

$$Re_{r_o} = 4Re/\xi \tag{40}$$

which is deduced from Eqs. (4c) and (13). The curve shows that a minimum value of $Re_{r_o} = 8.4875 \times 10^3$ is required to make the boundary layer unstable at a value $\xi_{tr} = 0.33$, with $n = 2$ being the mode to be amplified. The corresponding location of onset of instability can be computed by using Eq. (4c),

$$x_{tr} = \frac{1}{16}\xi_{tr}^2 (Re_{r_o})_{\min} r_o = 57.77 r_o$$

At a higher value of Re_{r_o}, the value ξ_{tr} shifts to a lower value on the left branch of the critical curve in Fig. 7, and the location of onset of instability x_{tr} can be calculated in a similar manner. For example, $\xi_{tr} = 0.1$ at $Re_{r_o} = 1.528 \times 10^4$, the resulting position of onset of instability is shifted upstream to $x_{tr} = 9.55 r_o$ and the excited mode is still $n = 2$.

In the case of small ξ, such as that for a cylinder of large radius or for a flat plate, it is preferable to use Fig. 6 instead of Fig. 7 to determine the condition for the onset of instability.

Spinning Cylinder

The spin motion introduces an additional mean flow in the tangential direction, whose profile can be obtained by solving Eq. (9) with boundary conditions (10) and (11) after the axial velocity has been computed from Eq. (8). Plotted in Fig. 8 are typical tangential velocity profiles at different values of ξ, obtained for $s = 1$, i.e., for the case in which the tangential velocity at the surface is equal to the freestream axial velocity.

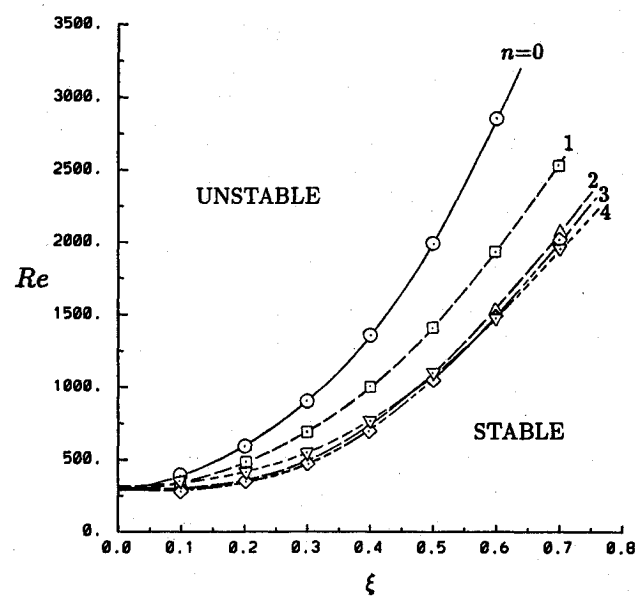

Fig. 11 Curves of the lowest Reynolds number vs the curvature factor ξ for axisymmetric and nonaxisymmetric disturbances with spin rate $s = 0.05$.

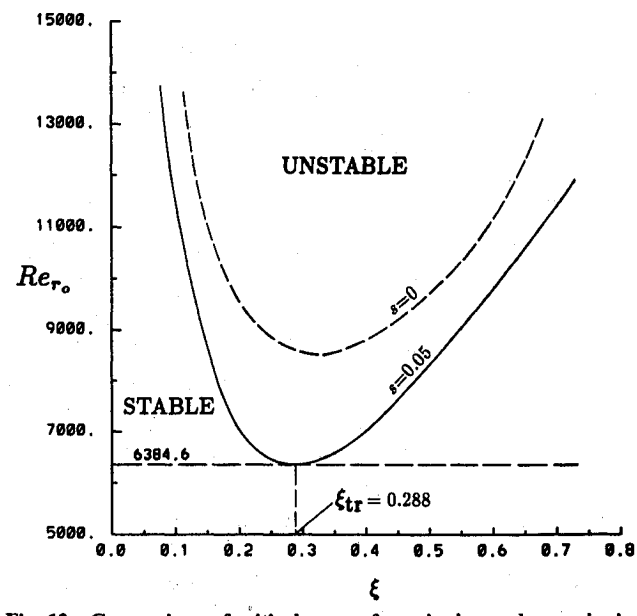

Fig. 12 Comparison of critical curves for spinning and nonspinning cylinders.

Since the axial velocity profiles are not influenced by the rotation, they remain the same as those shown in Fig. 3.

The effect of spin on boundary-layer instability can be observed by comparing the neutral stability curves plotted in Fig. 9 for $s=0.05$ with those in Fig. 5 for $s=0$, in which both sets of curves are computed at $\xi=0.3$. For this particular value of ξ, the critical Reynolds number drops from 6.39×10^2 in the nonspinning case to 4.8×10^2 in the presence of rotation with $s=0.05$, and the most unstable mode changes from $n=2$ to 3. It is noted that, for $\alpha\to0$, the lower branch of the neutral stability curve may become very close to the Re axis in the (α,Re) plane.[18] No computations have been made herein since such a small value of α may cause large numerical errors and result in an inaccurate solution.

The lowest Reynolds number that makes the $n=0$ mode unstable is plotted in Fig. 10 as a function of ξ. It shows that this mode is destabilized by increasing the spin rate. Such a behavior is found also in all other modes.

Plotted in Fig. 11 are the critical Reynolds numbers for the disturbed modes $n\leq4$ at different values of ξ for $s=0.05$. Along the critical curve, which is the lower envelope of all curves in Fig. 11, the most unstable mode varies rapidly from $n=0$ to 3 in a small range of ξ close to zero. It remains at $n=3$ for ξ up to 0.57 and changes to $n=4$ as ξ becomes >0.57.

Figure 12 shows the comparison of the critical curve for a spinning cylinder of $s=0.05$ with that for a nonspinning cylinder in the Re_{r_o} vs ξ diagram. It is found that the required value of Re_{r_o} to make the boundary layer unstable is equal to 6.3846×10^3 at a value $\xi_{tr}=0.288$, which gives an earlier location of onset of instability at $x_{tr}=33.1r_o$ as compared with $57.77r_o$ in the absence of a spin. In general, as can be seen in Fig. 12, the effect of spin is to destabilize the boundary-layer flow and to move the onset of instability upstream.

V. Conclusions

Numerical techniques have been successfully applied to study the stability of boundary layers on nonspinning and spinning circular cylinders whose axes are aligned with the oncoming flow. Authors were unable to find experimental data on stability of the boundary layer on a semi-infinite circular cylinder for comparison with the present calculations. However, the present results show that the Squire's theorem that $n=0$ is the most unstable mode is not valid for the flow along a circular cylinder with or without a spin, unless the cylinder radius is extremely large compared to the boundary-layer thickness. Transverse curvature has a stabilizing effect on both axisymmetric and nonaxisymmetric disturbances. Rotational motion of the cylinder destabilizes the flow and shifts the onset of instability toward the leading edge.

Acknowledgments

Funds for the support of this study have been allocated by the U.S. Air Force Office of Scientific Research (AFSC) under Contract F49620-88-C-0098. Part of the work of the first author was suppored by NASA Lewis Research Center under Grant NCC3-168. The authors are grateful to E. Laurien for his valuable advice and discussion on the application of the Chebyshev collocation spectral method.

References

[1]Young, A. D., "The Calculations of the Total and Skin-Friction Drags of Bodies of Revolution at Zero Incidence," British Aeronautical Research Council, London, R&M 1874, 1939.

[2]Jacob, M., and Dow, W. M., "Heat Transfer from a Cylindrical Surface to Air in Parallel Flow with and without an Unheated Starting Section," *ASME,* Vol. 68, No. 2, 1946.

[3]Seban, R. A., and Bond, R., "Skin-Friction and Heat Transfer Characteristics of a Laminar Boundary Layer on a Cylinder in Axial Incompressible Flow," *Journal of Aeronautical Science,* Vol. 18, No. 10, 1951, pp. 671–675.

[4]Glauert, M. B., and Lighthill, M. J., "The Axisymmetric Boundary Layer on a Long Thin Cylinder," *Proceedings of the Royal Society of London, Series A: Mathematical and Physical Sciences,* Vol. 230, 1955, pp. 188–203.

[5]Stewartson, K., "The Asymptotic Boundary Layer on a Circular Cylinder in Axial Compressible Flow," *Quarterly of Applied Mathematics,* Vol. 13, No. 2, 1955, pp. 113–122.

[6]Jaffe, N. A., and Okamura, T. T., "The Transverse Curvature Effect on the Incompressible Laminar Boundary Layer for Longitudinal Flow over a Cylinder," *ZAMP,* Vol. 19, Jan. 1968, pp. 564–574.

[7]Smith, A. M. O., and Clutter, D. W., "Solution of the Incompressible Laminar Boundary-Layer Equations," Douglas Aircraft Co., Long Beach, CA, Rept. ES 40446, July 1961.

[8]Schlichting, H., *Boundary Layer Theory,* 4th ed., McGraw-Hill, New York, 1960, pp. 188–192.

[9]Brown, F. N. M., "The Physical Model of Boundary Layer Transition," *Ninth Midwestern Mechanics Conference,* University of Wisconsin Press, Madison, WI, 1965.

[10]Knapp, C. F., and Roache, P. J., "A Combined Visual and Hot-Wire Anemometer Investigation of Boundary-Layer Transition," *AIAA Journal,* Vol. 6, No. 1, 1968, pp. 29–36.

[11]Kegelman, J. T., Nelson, R. C., and Mueller, T. J., "The Boundary Layer on an Axisymmetric Body With and Without Spin," *AIAA Journal,* Vol. 21, No. 11, 1983, pp. 1485–1491.

[12]Morris, P. J., and Byon, W., "The Stability of the Axisymmetric Boundary Layer on a Circular Cylinder," AIAA Paper 82-1012, June 1982.

[13]Laurien, E., "Lösung der Orr-Sommerfeld-Gleichung Für die Blasius'sche Grenzschichtströmung Mittels Chebyshev-Kollokation," DFVLR-AVA, Göttingen, Germany, IB 221-85 A 02, 1985.

[14]Gottlieb, D., Hussaini, M. Y., and Orszag, S. A., *Theory and Applications of Spectral Methods,* Society for Industrial and Applied Mathematics, Philadelphia, PA, 1984, pp. 1–54.

[15]Ouazzani, J., and Peyret, R., "A Pseudo-Spectral Solution of Binary Gas Mixtrue Flows," *Proceedings of the Fifth GAMM Conference on Numerical Methods in Fluid Mechanics,* Vieweg, Wiesbaden, Germany, 1984, pp. 275–282.

[16]Jordinson, R., "The Flat Plate Boundary Layer. Part 1. Numerical Integration of the Orr-Sommerfeld Equation," *Journal of Fluid Mechanics,* Vol. 43, Pt. 4, 1970, pp. 801–811.

[17]Richtmeyer, R. D., *Difference Methods for Initial Value Problems,* Interscience, New York, 1957, pp. 198–201, 275–282.

[18]Pai, S. I., "On the Stability of Two-Dimensional Laminar Jet Flow of Gas," *Journal of Aeronautical Science,* Vol. 18, 1951, pp. 731–742.

Walter B. Sturek
Associate Editor